



Modeling the haloperoxidases: Reversible oxygen atom transfer between bromide ion and an oxo-Mn(V) porphyrin

Dorothee Lahaye, John T. Groves *

Department of Chemistry, Princeton University, Princeton, NJ 08544, United States

Received 1 June 2007; received in revised form 9 July 2007; accepted 12 July 2007

Available online 21 July 2007

This paper is dedicated to the fond memory of Edward I. Stiefel, colleague, collaborator and friend.

Abstract

The manganese *meso*-dimethylimidazolium porphyrin complex Mn(III)[TDMImP] reacted with HOBr/OBr⁻ to generate the corresponding oxo-Mn(V)[TDMImP] species. The rate of this process accelerated with increasing pH. A forward rate constant, k_{for} , of $1.65 \times 10^6 \text{ M}^{-1} \text{ s}^{-1}$ was determined at pH 8. Under these conditions, the oxo-Mn(V) species is short-lived and is transformed into the corresponding oxo-Mn(IV) complex. A first-order rate constant, k_{obs} , of 0.66 s^{-1} was found for this reduction process at pH 8. The mechanism of this reduction process, which was dependent on bromide ion, appeared to proceed via an intermediate Mn(III)–O–Br complex. Thus, both a fast, reversible Mn(III)–O–Br bond heterolysis and a slower homolytic pathway occur in parallel in this system. The reverse oxidation reaction between oxo-Mn(V)[TDMImP] and bromide was investigated as a function of pH. The rate of this oxo-transfer reaction ($k_{\text{rev}} = 1.4 \times 10^3 \text{ M}^{-1} \text{ s}^{-1}$ at pH 8) markedly accelerated as the pH was lowered. The observed first-order dependence of the rate on [H⁺] indicates that the reactive species responsible for bromide oxidation is a protonated oxo-hydroxo complex and the stable species present in solution at high pH is dioxo-Mn(V)[TDMImP], [O=Mn(V)=O]⁻. The oxo-Mn(V) species retains nearly all of the oxidative driving force of the hypohalite. The equilibrium constant $K_{\text{equi}} = k_{\text{for}}/k_{\text{rev}}$ for the reversible process was determined at three different pH values ($K_{\text{equi}} = 1.15 \times 10^3$ at pH 8) allowing the measurement of the redox potentials E of oxo-Mn(V)/Mn(III) ($E = 1.01 \text{ V}$ at pH 8). The redox potential for this couple was extrapolated over the entire pH scale using the Nernst relationship and compared to those of the manganese 2- and 4-*meso*-*N*-methylpyridinium porphyrin couples oxo-Mn(V)[2-TMPyP]/Mn(III)[2-TMPyP], oxo-Mn(V)[4-TMPyP]/Mn(III)[4-TMPyP], OBr⁻/Br⁻ and H₂O₂/H₂O. Notably, the redox potential of oxo-Mn(V)/Mn(III) for the imidazolium porphyrin approaches that of H₂O₂/H₂O at low pH.

© 2007 Elsevier Inc. All rights reserved.

Keywords: Oxomanganese porphyrin; Bromoperoxidase; Chloroperoxidase; Redox potential; Cytochrome P450

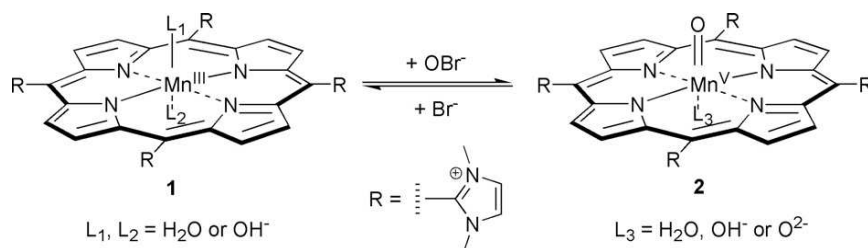
1. Introduction

Terminal metal-oxo species [M=O] are key reactive intermediates in many biological processes catalyzed by heme enzymes from the proton pumping apparatus of cytochrome oxidase to the oxygen activation and transfer reactions of cytochrome P450. The active species responsible for oxygen-transfer reactions in cytochrome P450 enzymes is considered to be an oxoFe(IV)-porphyrin π -cat-

ion radical (compound **1**) [1–5]. These enzymes are capable of catalyzing a wide variety of oxidation reactions with high selectivity including olefin epoxidations, C–H hydroxylations, *N*-dealkylations and *S*-oxidations. This rich reactivity has prompted sustained efforts toward the development of biomimetic oxidation catalysts. Iron and manganese porphyrins, in particular, are efficient catalysts and useful tools for studying structure–reactivity relationship in these catalytic and biological processes [1,2].

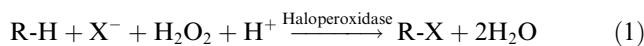
Haloperoxidases [6–8] are a class of enzymes that catalyze the oxidation of halide ions by hydrogen peroxide, with subsequent halogenation of organic substrates (Eq.

* Corresponding author. Tel.: +1 609 258 3593; fax: +1 609 258 0348.
E-mail address: jtgroves@princeton.edu (J.T. Groves).



Scheme 1. Reversible oxygen atom transfer between Mn(III)[TDMImP] (**1**) and hypobromite, and oxo-Mn(V)[TDMImP] (**2**) and bromide. The oxo-Mn(V) complex **2** refers to all high-valent species regardless of their protonation state. Specifically, **2** can exist as an oxo-aqua ($L_3 = \text{H}_2\text{O}$), an oxo-hydroxo ($L_3 = \text{OH}^-$) or a dioxo ($L_3 = \text{O}^{2-}$) species.

(1)). These processes, which play a major role in global organohalogen production [9,10], are thought to be important components of the chemical defense of the organisms that produce them. In addition, these halogenated natural products are of pharmacological interest due to their antifungal, antibacterial, antineoplastic, antiviral and anti-inflammatory activities [11].



The heme-containing haloperoxidases include lactoperoxidase, myeloperoxidase, chloroperoxidase (CPO), isolated from *Caldariomyces fumago* found in terrestrial systems [7,12–15], and FeHeme-BrPO from marine algal systems [16,17]. In the case of CPO, an iron(III) hydroperoxide (compound **0**) [18] and an iron(IV)porphyrin π -cation radical (compound **1**) have been detected and spectroscopically characterized [19,20]. It has been shown that chloride can react with the high-valent iron-oxo complex to produce an Fe(III)-OCl adduct. Freely diffusing HOCl [21–23] and the enzyme-bound Fe(III)-OCl adduct [24] are both considered as possible species responsible for delivering the “Cl⁺” equivalent. Kinetic studies involving FeHeme-BrPO indicate that the active brominating species is not enzyme bound, but is rather released into solution as seen by the accumulation of Br₃⁻ [16]. CPO is also one of the most functionally diverse of the known heme enzyme catalysts. In addition to catalyzing halogenation reactions, CPO exhibits peroxidase, catalase and cytochrome P-450 like activities. This enzyme is able to catalyze stereo- and regioselective sulfoxidation and epoxidation reactions [25–28].

There have been few studies devoted to the modeling of haloperoxidases with metalloporphyrin complexes. The first chloroperoxidase model was based on the association of NaClO₂ with an iron(III) deuteroporphyrin IX, generating HOCl in situ. This system was able to convert monochlorodimedone (MCD), a common substrate of haloperoxidases, to dichlorodimedone [29]. More recently, an iron(III) porphyrin complex containing a thiophenolato ligand coordinated to the Fe center was described by Woggon et al. [22]. Reaction intermediates were observed upon reaction of this model complex with H₂O₂/Cl⁻. Further, it was able to chlorinate MCD with high turnovers.

Manganese porphyrins have been extensively employed as biomimetic catalysts since the first detection of reactive oxo-Mn(V) intermediates [30,31]. Meunier et al. have described the chlorination of dimedone by the water-soluble porphyrin Mn(III)TMPS supported on a polyvinylpyridinium polymer [32]. The direct oxidation of bromide by oxygen atom transfer from oxo-Mn(V) complexes has been observed in our laboratory as well as the reverse reaction, i.e., oxidation of the Mn(III) porphyrin with HOBr/OBr⁻ [33,34]. Recently, Naruta et al. [35] reported the formation and characterization of a dinuclear oxo-Mn(V) porphyrin complex. Upon protonation, this high-valent species quantitatively oxidized Cl⁻ into OCl⁻.

In this paper, the oxidation of the manganese *meso*-dimethylimidazolium porphyrin complex Mn(III)[TDMImP] (**1**), with HOBr/OBr⁻ to produce an oxo-Mn(V)[TDMImP] complex **2** and the reverse reaction, oxidation of bromide with the high-valent species **2** to regenerate **1**, are investigated (Scheme 1). With this highly electron-deficient porphyrin ligand, **1** displays a reactivity that is significantly different from those observed for the isomeric *meso*-*N*-methylpyridyl porphyrins Mn(III)[2-TMPyP] (**3**) and Mn(III)[4-TMPyP] (**4**). Mechanisms explaining the reactivity of **1** are elucidated and equilibrium constants K_{equi} for oxo-transfer are measured, leading to the determination of the redox potential of the oxo-Mn(V) **2**/Mn(III) **1** couple over the entire pH range.

2. Materials and methods

2.1. Materials

Milli-Q water was used throughout the study. All buffers were prepared fresh daily and all the chemicals were of the best available purity. All oxidants (oxone, *t*-butyl hydroperoxide and NaOCl) were purchased from Aldrich. The peroxysulfate concentration of oxone was determined by iodometric titration. The active component of *t*-butyl hydroperoxide was determined by iodometric titration with sodium thiosulfate. Sodium hypochlorite was standardized spectrophotometrically [36]. Sodium bromide, sodium perchlorate and phenolsulfonephthalein were obtained from Aldrich and were used as received. Solutions of HOBr/

OBr⁻ were prepared by mixing sodium hypochlorite with sodium bromide under slightly basic conditions. A 5% excess of sodium bromide was employed to ensure full conversion of hypochlorite to hypobromite. The concentrations of HOBr/OBr⁻ solutions were standardized spectrophotometrically [36]. The HOBr/OBr⁻ solutions were then diluted in the appropriate buffer to obtain the desired pH. 5,10,15,20-tetrakis[1,3-*N,N*-dimethylimidazol-2-yl]porphyrinato manganese(III) chloride, Mn(III)[TDMImP]Cl (**1-Cl**), was synthesized according to the literature procedures [37,38].

2.2. Instrumentation

UV–Vis spectral measurements were carried out on a Hewlett-Packard 8453 diode-array spectrophotometer at room temperature. Stopped-flow experiments were performed with a Hi-Tech SF-61 DX2 double-mixing instrument with a 1 cm path length, the temperature being regulated with a thermostat bath ISOTEMP 1016 S from Fischer Scientific. ¹H NMR spectra were recorded on a 500 MHz Varian INOVA spectrometer. EPR experiments were recorded on a Bruker Elexys 580 X-band CW-EPR system with dual cavity mode. Cryogenic temperatures were obtained with a liquid helium cryostat.

2.3. Bromination of phenol red by UV–Vis spectroscopy

In a UV cell was placed 0.042 mL of a 1 mM solution of porphyrin **1**, 1.05 mL of a 20 mM solution of NaBr and 2.76 mL of a 10 mM phosphate buffer at pH 7.4. At $t = 0$, 0.042 mL of a 20 mM oxone solution was added followed by 0.105 mL of a 1 mM solution of phenol red at $t \geq 10$ s. The final concentrations for each species are as follows: [1] = 0.0105 mM, [NaBr] = 5.25 mM, [oxone] = 0.0105 mM and [phenol red] = 0.0263 mM. For the experiment without porphyrin **1**, 2.80 mL of buffer was added.

2.4. Stopped-flow experiments

The porphyrin oxidations with HOBr/OBr⁻ were carried out in the single-mixing mode under the diode-array or single wavelength mode. The first syringe was filled with the porphyrin complex **1** and the second one was filled with the oxidant (HOBr/OBr⁻, oxone or *t*-BuOOH), both dissolved in the same buffer at the chosen pH. Equal volumes of the two reactants were quickly mixed. The concentrations in porphyrin complex and oxidant were then divided by two. The bromide oxidation reactions were performed using the double-mixing mode. In a first push, the manganese porphyrin complex **1** was mixed with an equal volume of oxone, then, following an aging time (varies with pH), the bromide solution was added in a second push. The concentrations in porphyrin complex and oxone are divided by four and the bromide concentration is divided by two. The concentrations reported are the final concentrations. Each

experiment was carried out in duplicate or triplicate unless otherwise noted. All the experiments were performed in a buffer at $T = 22.2 \pm 0.2$ °C unless otherwise noted. The data were analyzed using the programs KinetAsyst 3.11 or Specfit/32 by monitoring the changes in absorbance at the wavelength of choice.

2.5. pK_a determination

The pK_a values corresponding to the successive deprotonation of the two water molecules axially bound to the manganese porphyrin were determined spectroscopically. The absorption spectrum of the Mn(III) complex **1** was taken at various pH values between pH 4.3 and 11.3 in a 10 mM Tris solution or between 3.1 and 10.3 in a 10 mM phosphate solution, while keeping the porphyrin concentration constant at 0.01 mM. For each measurement, a stable pH was observed even outside the buffer window. The absorption spectra were analyzed using the program Specfit/32. The pK_a values were determined by fitting the changes in absorbance with pH to a theoretical curve for the dissociation of a diprotic acid.

2.6. EPR experiments

The EPR sample was prepared by dissolving **1** in MeOH/pH 8 phosphate buffer (1:2) ([1] ≈ 2 mM), to which about 10 equiv of *t*-butyl hydroperoxide were added. A portion of the solution prepared (200 μL) was transferred to the EPR tubes and immediately frozen in liquid N₂. The temperature was set at 5 K and the power attenuation was at 20 dB in the perpendicular mode.

3. Results

3.1. Oxidation of Mn(III)[TDMImP] (**1**) with HOBr/OBr⁻ at pH 8

The oxidation of Mn(III)[TDMImP] (**1**) with HOBr/OBr⁻ was studied by diode-array stopped-flow spectroscopy in 10 mM pH 8 phosphate buffer (Fig. 1). The addition of 0.0625 mM of HOBr/OBr⁻ to 0.0128 mM of Mn(III)[TDMImP] (**1**) ($\lambda_{\max} = 442$ nm) fully generated the oxo-Mn(V) complex **2** with a Soret band at $\lambda = 425$ nm. Clean isosbestic points were observed at 374, 434, 521, 552.5, 570 and 584 nm. Similar spectral features were observed for the oxidation of porphyrin **1** with oxone under similar conditions. A second-order fit was applied to the absorbance changes at 425 nm for the conversion of **1** to **2**. The apparent second-order rate constant, k_{for} , was determined to be $1.65 \times 10^6 \text{ M}^{-1} \text{ s}^{-1}$ at pH 8. With oxone, a k_{for} value of $1.53 \times 10^6 \text{ M}^{-1} \text{ s}^{-1}$ was obtained. The high-valent species **2** was characterized by ¹H NMR spectroscopy following oxidation of **1** with oxone under slightly basic conditions. The spectrum displayed sharp proton resonances characteristic of a diamagnetic compound with a

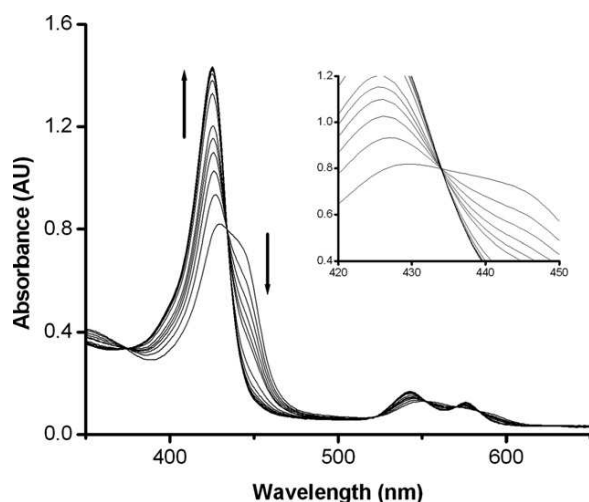


Fig. 1. Time-resolved spectra for the reaction between 0.0128 mM **1** and 0.0625 mM HOBr/OBr⁻ in 10 mM pH 8 phosphate buffer over 0.2 s. The oxo-Mn(V) **2** reached its highest absorbance in about 0.11 s. Isosbestic points are observed at 434, 374, 521, 552.5, 570 and 584 nm. The apparent second-order rate constant, k_{for} , for the formation of species **2** was estimated to be $1.65 \times 10^6 \text{ M}^{-1} \text{ s}^{-1}$. Inset: zoom on the isosbestic point at 434 nm. (100 scans, traces 1 in 5 shown.)

low-spin d^2 configuration as previously observed with oxo-Mn(V)[2-TMPyP] (**5**) [39].

3.2. pH dependence of the oxidation of Mn(III) [TDMImP] (**1**) with HOBr/OBr⁻

The oxidation of **1** with HOBr/OBr⁻ was also studied at other pH values to determine the pH dependence of the reaction. For these reactions, a higher oxidant concentration was employed with [HOBr/OBr⁻] = 0.26 mM. In pH 6.8 (Fig. S1) and 7.2 10 mM phosphate buffers, the same high-valent species **2** was formed. As the pH was lowered, a decrease in the maximum absorbance of species **2** was observed. About 90% of **2** were formed at pH 7.2, while only about 80% was generated at pH 6.8. A two-exponential fit was applied to the traces at 425 nm to account for both the formation of the oxo-Mn(V) complex **2** (k_{obs1}) and its decay (k_{obs2}). The apparent second-order rate constants, k_{for} , for these oxidation reactions were determined by dividing the k_{obs1} values by the initial concentration in oxidant. The calculated values are: $k_{\text{for}} = 2.6 \times 10^5 \text{ M}^{-1} \text{ s}^{-1}$ at pH 7.2 and $k_{\text{for}} = 7.6 \times 10^4 \text{ M}^{-1} \text{ s}^{-1}$ at pH 6.8. Log k_{for} was plotted as a function of pH (Fig. 2). A slope of 1.1 was obtained, which suggests the loss of a proton in the rate-determining step of the oxidation reaction.

3.3. Stability of the high-valent oxo-Mn(V) complex **2**

At pH 8, as soon as the oxo-Mn(V) complex **2** was fully generated by addition of 5 equiv. HOBr/OBr⁻, it quickly decayed to form a new species **6** with a Soret at 424 nm and a shoulder at 390 nm (Fig. 3). A species with identical

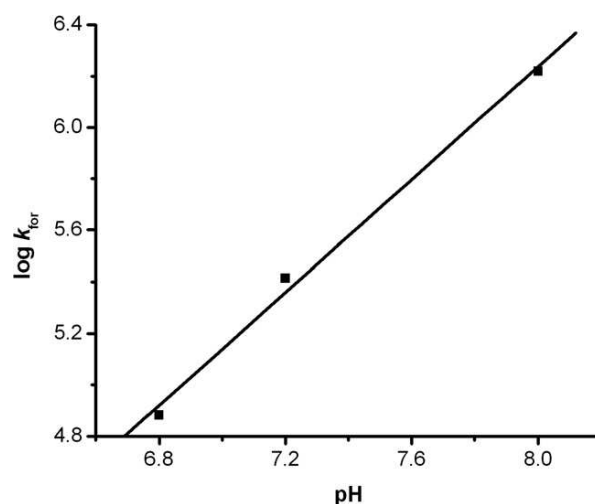


Fig. 2. Plot of log k_{for} vs pH for the formation of the high-valent species **2** by oxidation of porphyrin **1** with HOBr/OBr⁻ in 10 mM phosphate buffer. A slope of 1.1 is obtained ($R^2 = 0.9944$).

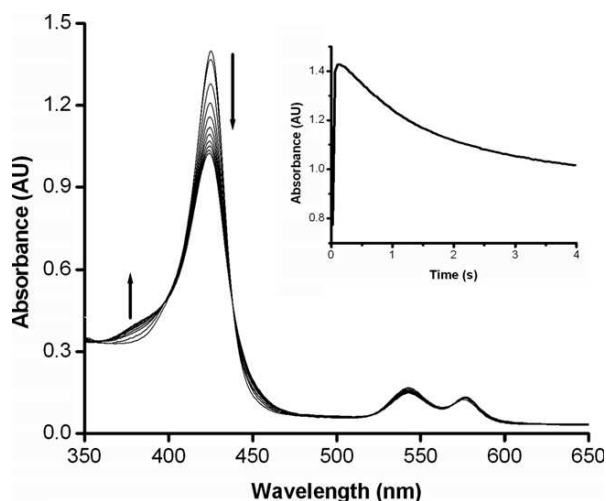


Fig. 3. Time-resolved spectra for the reaction between 0.0128 mM **1** and 0.0625 mM HOBr/OBr⁻ in 10 mM pH 8 phosphate buffer over 4 s. The high-valent species **2** was formed in about 0.11 s (Fig. 1), then it decayed to form the oxo-Mn(IV) species **6** as seen by the decrease in intensity and slight blue-shift of the Soret band and by the formation of a shoulder around 390 nm. Inset: trace at 425 nm, corresponding to λ_{max} of **2**. (100 scans, 12 traces shown.)

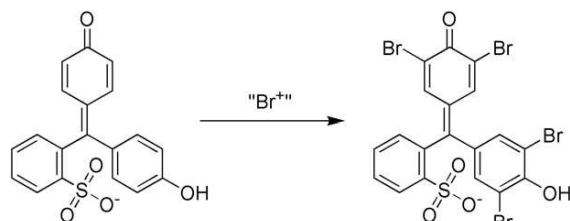
spectral features was generated by oxidation of **1** with *t*-BuOOH (1 equiv.) at pH 8 (Fig. S2). The EPR spectra of the high-valent species displayed specific characteristics of a high-spin, monomeric d^3 Mn(IV) species, i.e. a strong broad resonance at $g_{\perp} = 3.7$ and a weak signal at $g_{\parallel} = 1.96$. Accordingly, the initially-formed oxo-Mn(V) complex **2** quickly decayed under these conditions to generate the oxo-Mn(IV) species **6**. By contrast, the oxo-Mn(V) species **2** generated with 5 equiv. of oxone at pH 8 in the absence of bromide ion did not show any signs of fast decay. The first-order rate constant for the conversion of **2** to **6** was estimated to be 0.66 s^{-1} .

3.4. Reaction of the oxo-Mn(V) complex **2** with bromide: diagnostic characterization of OBr⁻ formation

To monitor bromide oxidation by the high-valent species **2**, and thus the formation of OBr⁻, the oxidation reaction was studied by UV–Vis spectroscopy in the presence of phenol red. This phenolic dye is commonly used as a standard assay for haloperoxidase activity [40]. In the presence of HOBr, Br₂ or Br₃⁻, phenol red is easily tetrabrominated to form bromophenol blue (Scheme 2). Under neutral conditions, a red shift from 441 nm, characteristic of phenol red, to 590 nm, characteristic of bromophenol blue, is observed, along with a color change from orange-red to purple. The oxidation of bromide by the oxo-Mn(V) complex **2**, formed by reaction of Mn(III)[TDMImP] (**1**) with oxone (KHSO₅), was studied in 10 mM pH 7.4 phosphate buffer at room temperature. A blank experiment was also performed with no porphyrin present in the solution. The addition of 0.105 mM of oxone to a solution containing 5.25 mM of NaBr and 0.0105 mM of **1** in a 10 mM pH 7.4 phosphate buffer generated the oxo-Mn(V) complex **2**. Following the addition of 0.263 mM of phenol red, the solution turned purple instantaneously and a new absorption band appeared at 590 nm indicating the formation of bromophenol blue. At the same time, the high-valent species was reduced to the Mn(III) state (Fig. S3). When the reaction was realized without Mn(III)[TDMImP] **1**, the bromination of phenol red was much slower (Fig. S4). A $\lambda_{\text{max}} = 590$ nm was only achieved after 290 s of reaction. The bromination of phenol red was about 28 times faster when the Mn(III) porphyrin complex **1** was present in the system. The formation of hypobromite was thus accelerated by the presence of the manganese porphyrin **1**. Therefore, Mn(III)[TDMImP] can act as a catalyst for bromide oxygenation.

3.5. Kinetics of bromide oxygenation

The oxidation of bromide by oxo-Mn(V)[TDMImP] (**2**) was investigated by stopped-flow spectroscopy at room temperature. The experiments were carried out in 10 mM phosphate buffer between pH 5.95 and 8, and in 10 mM acetate buffer at pH 5.6 and 5.2. All the solutions were adjusted to the same ionic strength with 100 mM sodium perchlorate, NaClO₄. The oxo-Mn(V) complex **2** was formed by mixing 0.007 mM of porphyrin **1** with



Scheme 2. Bromination of phenol red to generate bromophenol blue.

0.007 mM of oxone, then various concentrations of sodium bromide were added when the highest concentration of oxo-Mn(V) **2** was achieved. The sodium bromide concentrations were varied from 0.035 to 0.14 mM. Once sodium bromide was added, the oxo-Mn(V) complex **2** was reduced back to the Mn(III) state. At pH 6.8, an isosbestic point was observed at 434.5 nm, same wavelength as for the oxidation of **1** with HOBr/OBr⁻. The kinetic profiles were obtained by monitoring the disappearance of the oxo-Mn(V) complex **2** at 425 nm. A one-exponential equation was applied to the kinetic data except at pH 7.6 and 8 where a two-exponential equation was applied to account for side reactions competing with the oxo-transfer reaction. The trace at 425 nm for the decay of the oxo-Mn(V) complex **2** upon addition of 0.14 mM of bromide at pH 5.2 and the one-exponential fit applied can be seen in Fig. 4. The oxidation reaction was found to be first-order in sodium bromide at each pH studied (Fig. S5), the observed rate constant, k_{obs} , increasing linearly with [NaBr]. The apparent second-order rate constants, k_{rev} , were calculated from the linear slopes of the plots k_{obs} vs [NaBr] (Fig. 5). The values for k_{rev} vary from $1.4 \times 10^3 \text{ M}^{-1} \text{ s}^{-1}$ at pH 8 to $10^6 \text{ M}^{-1} \text{ s}^{-1}$ at pH 5.2. The pH dependence of k_{rev} is plotted in Fig. 6. The rate of the reaction increases as the pH is lowered. A one-proton dependence was observed over the pH range studied.

3.6. Determination of the redox potential of the oxo-Mn(V) 2/Mn(III) 1 couple

The second-order rate constants k_{for} and k_{rev} corresponding to the forward reaction (Mn(III)[TDMImP] (**1**) + HOBr/Br⁻) and reverse reaction (oxo-Mn(V)-

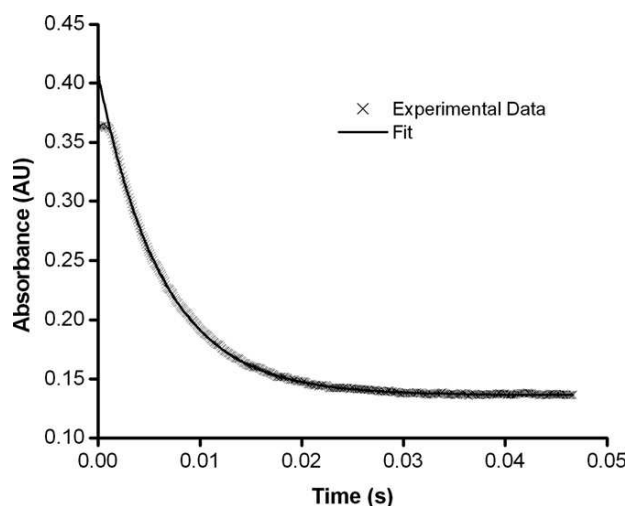


Fig. 4. Decay of the absorbance at 425 nm upon addition of 0.14 mM NaBr to a solution of oxo-Mn(V) **2** formed by mixing 0.007 mM porphyrin **1** with 0.007 mM oxone in 10 mM pH 5.2 acetate buffer. A one-exponential fit was applied giving the observed first-order rate constant, $k_{\text{obs}} = 160 \text{ s}^{-1}$.

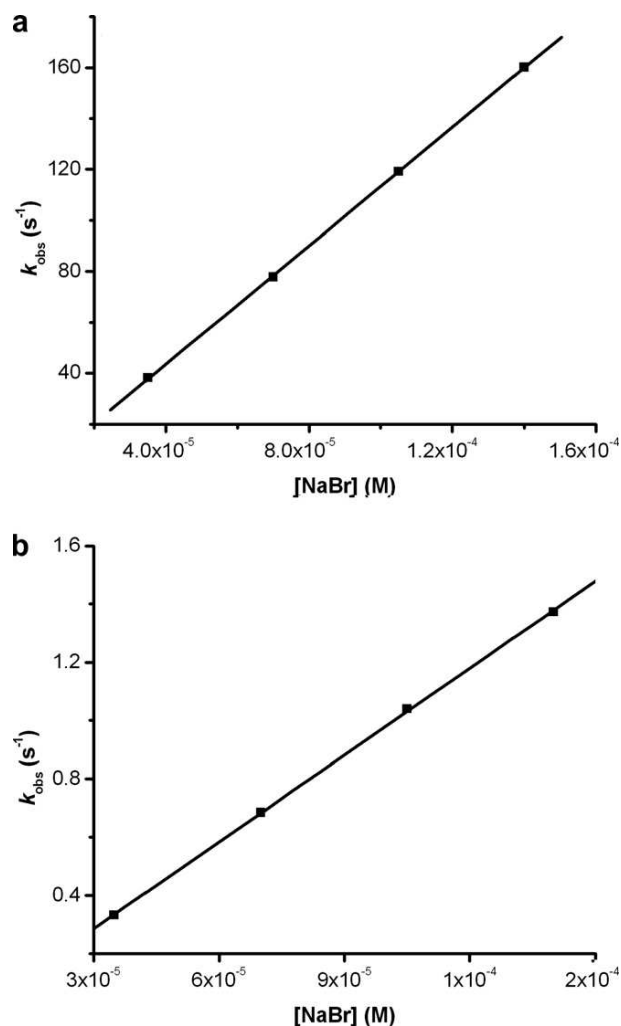


Fig. 5. Plots of the pseudo-first order rate constant k_{obs} as a function of $[\text{NaBr}]$ for the reaction between oxo-Mn(V) **2** and Br^- in (a) 10 mM pH 5.2 acetate buffer and (b) 10 mM pH 7.2 phosphate buffer. Bromide concentration was varied from 0.035 to 0.14 mM. The apparent second-order rate constants k_{rev} , corresponding to the slopes of the plots, were determined to be $1.16 \times 10^6 \text{ M}^{-1} \text{ s}^{-1}$ ($R^2 = 0.999$) at pH 5.2 and $9.94 \times 10^3 \text{ M}^{-1} \text{ s}^{-1}$ at pH 7.2 ($R^2 = 0.999$).

$[\text{TDMImP}]$ (**2**) + Br^-) have been determined at pH 6.8, 7.2 and 8. The equilibrium constant, K_{equi} , for this interconversion was then calculated at these three pH values with $K_{\text{equi}} = k_{\text{for}}/k_{\text{rev}}$. These values are gathered in Table 1. The K_{equi} values increase with pH. This clearly demonstrates that porphyrin oxidation with HOBr/OBr^- is thermodynamically more favorable under basic conditions and that bromide oxidation by the oxo-Mn(V) complex is faster under acidic conditions. The equilibrium constants K_{equi} obtained allowed us to calculate the redox potential $E_{2/1}$ for the oxo-Mn(V) **2**/Mn(III) **1** couple as a function of pH. The $E_{2/1}$ redox potentials were determined as follows (Eqs. (2) and (3)). The calculated $E_{2/1}$ values are 1.13, 1.09 and 1.01 V at pH 6.8, 7.2 and 8, respectively.

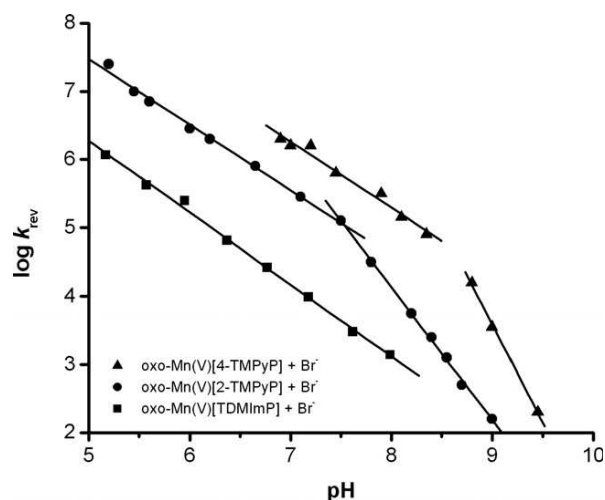


Fig. 6. Plot of $\log k_{\text{rev}}$ vs pH for the oxidation of bromide with oxo-Mn(V)[TDMImP] (**2**) (■), oxo-Mn(V)[2-TMPyP] (**5**) (●) and oxo-Mn(V)[4-TMPyP] (**7**) (▲). A slope of -1.05 was obtained for $\log k_{\text{rev}}$ vs pH for oxo-Mn(V)[TDMImP] (**2**).

Table 1

Equilibrium constants K_{equi} for the reversible reaction between Mn(III)[TDMImP] (**1**)/ OBr^- and oxo-Mn(V)[TDMImP] (**2**)/ Br^-

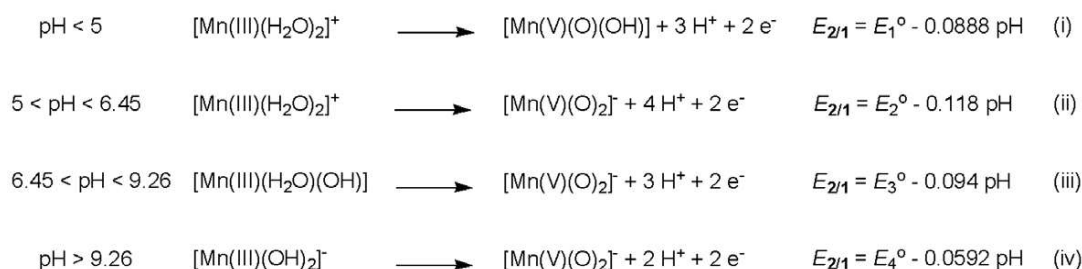
pH	$k_{\text{for}} (\text{M}^{-1} \text{ s}^{-1})$ Mn(III) + OBr^-	$k_{\text{rev}} (\text{M}^{-1} \text{ s}^{-1})$ Mn(V) = O + Br^-	K_{equi} ($k_{\text{for}}/k_{\text{rev}}$)
6.8	7.60×10^4	2.64×10^4	2.9
7.2	2.60×10^5	9.94×10^3	28
8	1.65×10^6	1.43×10^3	1155

$$\Delta E = \frac{0.0592}{n} \log K_{\text{equi}} \quad (2)$$

$$n = 2 \quad \text{and} \quad \Delta E = E_{\text{OBr}^-/\text{Br}^-} - E_{2/1}$$

$$E_{2/1} = E_{\text{OBr}^-/\text{Br}^-} - 0.0296 \log K_{\text{equi}} \quad (3)$$

From these experimental data and with knowledge of the approximate $\text{p}K_{\text{a}}$ values of the two species involved, the redox potential $E_{2/1}$ was extrapolated over the entire pH scale using the Nernst equation. In the case of complex **1**, the $\text{p}K_{\text{a}}$ values corresponding to the successive deprotonations of the water molecules coordinated to the manganese(III) center were determined to be 6.45 ± 0.17 and 9.26 ± 0.04 in a phosphate solution and 7.82 ± 0.04 and 8.78 ± 0.05 in a Tris solution. The difference in $\text{p}K_{\text{a}}$ values can be attributed to the binding of phosphate to the manganese center. As all the experiments leading to the determination of the equilibrium constants were performed in phosphate buffer, the first set of $\text{p}K_{\text{a}}$ values determined was employed for the extrapolation of the redox potential vs pH. For the oxo-Mn(V) complex **2**, the $\text{p}K_{\text{a}2}$ value, corresponding to the equilibrium between the oxo-hydroxo-Mn(V) and the dioxo-Mn(V) complexes, was set at 5. This value was determined based on the following spectrophotometric data. The oxo-Mn(V) complex, generated by the oxidation of Mn(III) porphyrin **1** with oxone, could be



Scheme 3. Half-reactions for the couple oxo-Mn(V) **2**/Mn(III) **1** as a function of pH and corresponding Nernst half-equations.

observed from pH 4.6 to 14 without any spectral changes ($\lambda_{\text{max}} = 425 \text{ nm}$). However, below pH 4.6, the high-valent complex could no longer be detected, even when employing large concentrations of oxidant. We then inferred that this change could be accounted for by the protonation of the dioxo-Mn(V) complex, the resulting oxo-hydroxo-Mn(V) being too unstable to be observed. With the data in hand, four half-reactions can be written between the Mn(III) complex **1** and the oxo-Mn(V) species **2** (Scheme 3). For each half-reaction corresponds a Nernst half-equation, the slope of which is dependent on the number of protons and electrons involved. In the case of half-reaction (iii) in Scheme 3, the slope was determined using the three experimental $E_{2/1}$ values previously obtained at pH 6.8, 7.2 and 8. A slope of 0.094 was found, which is close to the theoretical value of 0.0888 for a half-reaction involving three protons and two electrons. Fig. 7 shows the redox potential E vs pH diagram obtained for the couple oxo-Mn(V)[TDMImP] (**2**)/Mn(III)[TDMImP] (**1**), along with the following couples: oxo-Mn(V)[TDMImP] (**5**)/Mn(III)[TDMImP] (**3**), oxo-Mn(V)[TDMImP] (**7**)/Mn(III)[TDMImP] (**4**), OBr^-/Br^- and $\text{H}_2\text{O}_2/\text{H}_2\text{O}$.

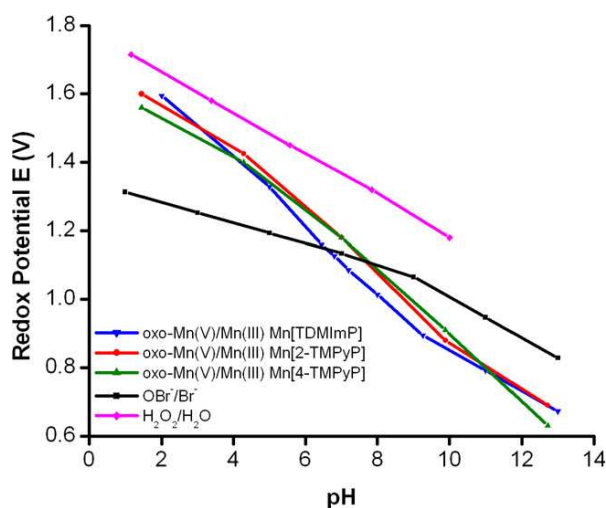


Fig. 7. Redox potential E (vs NHE) vs pH diagram for the following couples: $\text{H}_2\text{O}_2/\text{H}_2\text{O}$ (magenta), OBr^-/Br^- (black), oxo-Mn(V) (**7**)/Mn(III) (**4**) of Mn[4-TMPyP] (green), oxo-Mn(V) (**5**)/Mn(III) (**3**) of Mn[2-TMPyP] (red) and oxo-Mn(V) (**2**)/Mn(III) (**1**) of Mn[TDMImP] (blue). (For interpretation of the references to colour in this figure legend, the reader is referred to the web version of this article.)

4. Discussion

The fast, reversible oxygen transfer reaction between Mn(III)[TDMImP] (**1**)/ OBr^- and oxo-Mn(V)[TDMImP] (**2**)/ Br^- (Scheme 1) reported here and comparisons to similar reactions of the 2- and 4-*N*-methylpyridyl porphyrins we have previously described [33,34] have revealed much about the mechanism of oxidative catalysis. We have shown that the rate of formation of the high-valent oxo-Mn(V) complex **2** increases under basic conditions whereas the reverse process, the oxygen transfer reaction to substrates, is accelerated at low pH values. The determination of equilibrium constants for oxo-transfer to bromide has afforded a rare opportunity to place manganese porphyrin mediated oxygen transfer on an absolute energy scale. Notably, the results show that the reactive oxomanganese(V) porphyrin intermediates have retained nearly all of the thermodynamic driving force for oxygen transfer as the hypohalite that was used to generate them. Also, we have shown that the fast heterolytic cleavage of the O-Br bond in Mn(III)-O-Br to afford Mn(V)=O is accompanied by a slower, homolytic reaction that produces Mn(IV)=O. The various aspects of this haloperoxidase model reaction and, more generally, their relationships to oxometalloporphyrin reactivity, will be discussed below.

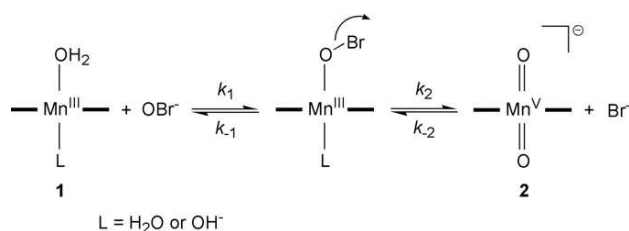
4.1. Oxidation of Mn(III)[TDMImP] (**1**) with HOBr/OBr^- : formation of an oxo-Mn(V) complex

A wide variety of catalytic systems involving metalloporphyrins and external oxidants have developed over the past three decades [1–4]. For the manganese porphyrin systems, reactive oxo-Mn(V) intermediates, first detected in our laboratory at low temperatures [30,31], were later evaluated kinetically by stopped-flow spectroscopy with Mn(III)[4-TMPyP] (**4**) [41] and characterized to have a singlet d^2 by ^1H NMR spectroscopy with the 2-pyridyl isomer [39]. Other oxo-Mn(V) complexes have been reported subsequently in both aqueous and organic solutions [33,42–44]. Oxo-Mn(V) complexes have also been characterized with other tetrapyrrole complexes such as corroles [45] and corrolazines [46].

Hypohalites in combination with manganese porphyrin catalysts have often been used in biomimetic oxygenation systems. Hypochlorite is a cheap, readily available and

strong oxidant. These systems, usually studied under biphasic conditions, have proven to be efficient for mediating epoxidation and hydroxylation reactions [47–49]. No high-valent species were observed in those cases, but it was proposed that hypochlorite could bind the Mn(III) center to form a Mn(III)-OCl adduct that, upon cleavage of the O-Cl bond, would yield an oxomanganese(V) complex [50,51]. Recently, we studied the oxidation of the water-soluble, *meso*-*N*-methylpyridyl porphyrin complexes Mn(III)[2-TMPyP] (**3**) and Mn(III)[4-TMPyP] (**4**) with hypochlorite, and successfully generated the corresponding oxo-Mn(V) complexes **5** and **7** in aqueous solutions [39,41]. An apparent second-order rate constant of $6.3 \times 10^5 \text{ M}^{-1} \text{ s}^{-1}$ was obtained at pH 7.4 for the oxidation of porphyrin **4** [41]. Few cases involving hypobromite, a slightly weaker oxidant than hypochlorite, have been reported [52,53]. The porphyrin complexes **3** and **4** were also reacted with this oxidant in aqueous solutions and an oxo-Mn(V) species was detected spectroscopically and kinetically characterized in both cases [33,34].

Oxidation of the *meso*-*N,N*-dimethylimidazolium porphyrin Mn(III)[TDMImP] (**1**) with HOBr/OBr⁻ generated an oxo-Mn(V) complex that was found to be distinctly more stable than **5** and **7**. Direct formation of the oxo-Mn(V) complex **2** from porphyrin **1** was observed with clear isosbestic points (Fig. 1). The oxo-Mn(V) complex **2** is presumably formed by heterolytic cleavage of the O-Br bond of an intermediate Mn(III)-O-Br complex, although the latter was not detected. This reaction is thermodynamically favored. Bromide is an excellent leaving group (pK_a of -9 for HBr [54]). Thus, using the Brønsted relationship, one expects bromide ion to be about 15 kcal/mol more stable than SO₄²⁻ ($pK_a = 1.96$), the product resulting from the O-O bond heterolytic cleavage of oxone. The proposed mechanism of formation of the high-valent oxo-Mn(V) complex **2** is shown below (Scheme 4). The oxidation reaction displays a strong pH dependence, the rate increasing with pH (Fig. 2). The same trend was observed with the *N*-methylpyridyl porphyrins **3** and **4**, although the second-order rate constant, k_{for} , for the oxidation of these complexes with HOBr/OBr⁻ was about one order of magnitude lower than with porphyrin **1** at pH 8 (Fig. S6) [34]. Mn(III)[TDMImP] (**1**) is therefore more readily oxidized than the two pyridyl porphyrins **3** and **4** despite the more electron withdrawing nature of the imidazolium substitu-

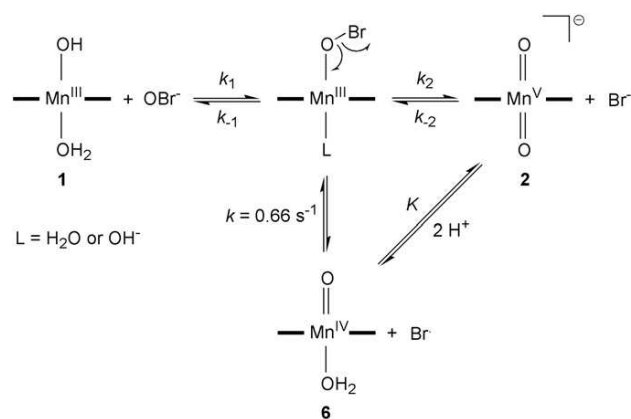


Scheme 4. Proposed mechanism for the oxidation of Mn(III)[TDMImP] (**1**) with HOBr/OBr⁻ to generate the oxo-Mn(V) complex **2**.

ent. As shown in Fig. 2, a proton is lost during the oxidation reaction. Under the reaction conditions employed for the experiments (pH ≤ 8), HOBr is the major species in solution. With a pK_a of 8.7, the proton loss could therefore come from the deprotonation of HOBr. A deprotonation of one of the ligands coordinated to the manganese complex in species **1** or in the intermediate Mn(III)-O-Br could also account for this observation.

At pH 8, the oxo-Mn(V) species **2** formed rapidly by the addition of 5 equiv. of HOBr/OBr⁻ and decayed within a few seconds affording the oxo-Mn(IV) complex **6**. The latter species, **6**, displayed higher stability than the oxo-Mn(V) species **2** under these conditions. The one-electron reduction observed is not due to the spontaneous decay of the high-valent species **2** since **2** produced by the oxidation of **1** with oxone did not decay in this manner. The only difference with the reaction carried out with oxone is the presence of bromide ion. In addition, the oxidation of Mn(III)[TDMImP] (**1**) with HOBr/OBr⁻ to form the oxo-Mn(V) complex **2** is reversible. We conclude, therefore, that re-addition of bromide at the oxo-moiety of the high-valent species **2** is dynamically reforming the Mn(III)-O-Br intermediate. This adduct does not regenerate the starting Mn(III) complex and the oxidant, as no absorption bands corresponding to the Mn(III) complex **1** were observed. However, the Mn(III)-O-Br complex can undergo a homolytic cleavage of the O-Br bond generating the oxo-Mn(IV) complex **6** (Scheme 5). Interestingly, homolytic Cl-O-Fe(heme) decomposition has been invoked by Ortiz de Montellano recently to explain the mesoheme chlorination observed for the peroxidase from *Arthromyces ramosus* [55].

This homolytic pathway is apparently thermodynamically favored. With a bond dissociation energy (BDE) of 87.6 kcal/mol for H-Br [54], Br⁻ is 16.4 kcal/mol more stable than *t*-butyloxy radical with a bond dissociation energy of 104 kcal/mole reported for the O-H bond of *t*-butanol [56]. *t*-Butyloxy radical is the product resulting from the O-O bond homolysis of *t*-butylhydroperoxide, an oxidant



Scheme 5. Mechanism of formation of the oxo-Mn(IV) complex **6** at pH 8.

known to generate an oxo-Mn(IV) species as discussed above. The two-step reduction of the oxo-Mn(V) complex **2** generating the oxo-Mn(IV) complex **6** can be written as an equilibrium between the two high-valent species as shown in Scheme 6. The equilibrium constant for this process is related to the potentials of the two couples involved: oxo-Mn(V) **2**/oxo-Mn(IV) **6** and Br[•]/Br⁻. The potential for Br[•]/Br⁻ is $E^0 = 1.92$ V [57]. To explain the chemistry observed, a higher potential for oxo-Mn(V) **2**/oxo-Mn(IV) **6** (E_6^0) is thus expected. The E_6^0 potential can be calculated as shown in Scheme 6. An E_6^0 value of 2.20 V was found. Since the E_6^0 for oxo-Mn(V) **2**/oxo-Mn(IV) **6** is higher than that of Br[•]/Br⁻, the one-electron reduction of the oxo-Mn(V) complex **2** is thermodynamically favored. The ΔG^0 value for the reaction was determined to be -6.5 kcal/mol. We note that [(aq)Cr(IV) = O]²⁺ has also been shown to oxidize bromide ion via a one-electron oxidation [58].

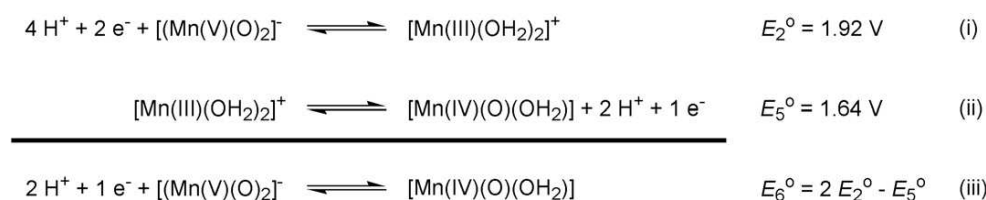
4.2. Comparison of bromide oxygenation by oxo-Mn(V) complexes **2**, **5** and **7**

The oxygenation of bromide has previously been investigated with the high-valent species oxo-Mn(V)[4-TMPyP] (**7**) and oxo-Mn(V)[2-TMPyP] (**5**) [33,34]. The profound pH dependence observed (Fig. 6) led us to conclude that the rate of oxo-transfer in these systems was controlled by equilibria between the various protonated states, dioxo-, oxo-hydroxo- and oxo-aqua-, of the high-valent manganese(V) species. We further concluded that the active oxo-Mn(V) species involved in the oxygen transfer was the oxo-aqua-Mn(V) complex (Scheme 7). The proposed mechanism was supported by DFT calculations [34] that have located the pertinent pK_a values and indi-

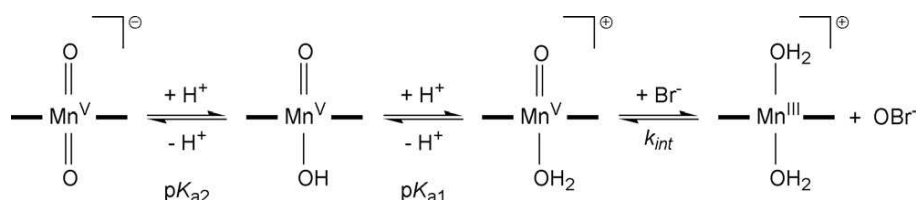
cated that the successive protonations of the oxo-Mn(V) species lowered the energy gaps between the singlet ground state (S) and the triplet (T) and quintet (Q) excited states and also increased the electron affinity. The higher reactivity observed at low pH appears to be related to the T and Q spin states becoming more accessible, this phenomenon being associated with a weakening of the oxo-Mn bond since the transition state for the reaction occurs near a T-Q energy crossing.

The reaction between oxo-Mn(V) **2** and Br⁻ has been characterized in the present work as a two-electron reduction of the high-valent oxo-Mn(V) species to the Mn(III) complex **1** upon nucleophilic addition of bromide to the oxo-Mn(V) oxygen and concomitant formation of coordinated BrO⁻. This oxygen transfer reaction, which is analogous to olefin epoxidation or *S*-oxygenation, was observed to decrease in rate by 3 orders of magnitude at higher pH. For oxo-Mn(V)[TDMImP] (**2**), the rate constant showed first-order dependence in [H⁺] over the entire pH range studied (5.2 < pH < 8), in contrast to the behavior of **5** and **7** that showed distinct biphasic behavior (Fig. 6). A low pK_{a2} value is inferred for the equilibrium between the oxo-hydroxo-Mn(V) and the dioxo-Mn(V) complexes ($pK_{a2} \leq 5$) in **2**. This is the result of the higher acidity of coordinated hydroxide for the imidazolyl porphyrin vs the 2- and 4-*N*-methylpyridyl complexes, resulting from the presence of positive charges lying closer to the metal center.

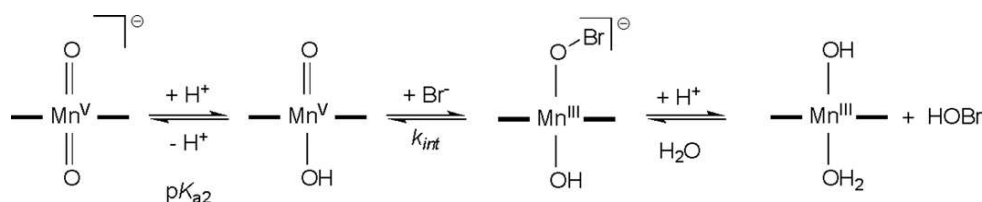
Under the present experimental conditions, the very stable high-valent manganese(V) species that is present at high pH is the dioxo-Mn(V) porphyrin complex, [O=Mn(V)=O]⁻ as we have previously discussed [33,34]. The likely presence of such a deprotonated dioxo form for Mn(V) at high pH was first inferred by Su et al. on



Scheme 6. Determination of the oxo-Mn(V) **2**/oxo-Mn(IV) **6** potential E_6^0 . The potentials for the Mn(IV) **6**/Mn(III) **1** couple (vs NHE) were determined by cyclic voltammetry using a three-electrode cell (vs Ag/AgCl) at pH 8.7, 9.5 and 13.6. A potential vs pH diagram based on the protonation state of each species involved was constructed from this data, allowing the determination of the potential E_5^0 . The potential E_2^0 was previously determined in Scheme 3 (ii).



Scheme 7. Proposed mechanism for the oxidation of bromide by the oxo-Mn(V) complexes oxo-Mn(V)[4-TMPyP] (**7**) and oxo-Mn(V)[2-TMPyP] (**5**). The active form for both high-valent species is the oxo-aqua-Mn(V) complex while the stable form is dioxo-Mn(V).



Scheme 8. Proposed mechanism for the oxidation of bromide with oxo-Mn(V)[TDMImP] (2).

the basis of electrochemical measurements [59]. It has very recently been reported by Song et al. [44] that manganese(V) porphyrins prepared according to the method of Watanabe [31] are also stabilized by excess base in non-aqueous solvents. Our results [33,34] show that the high stability and slow oxo-Mn exchange rates reported indicate that dioxo-Mn(V) complexes are formed under those conditions as well.

The data show that oxo-Mn(V)[TDMImP] (2) is about 1–2 orders of magnitude less reactive than oxo-Mn(V)[2-TMPyP] (5) and 2–3 orders compared to the 4-pyridyl-isomer 7 at a given pH. The first-order proton dependence observed for oxo-transfer from 2 can be interpreted in at least two ways. The most straightforward interpretation for the low reactivity of 2 is a rate-limiting, nucleophilic attack by bromide ion on the oxo-hydroxo-Mn(V) form (Scheme 8). By contrast, the main reaction pathway for 5 and 7 seems to involve the oxo-aqua form due to the lower acidity of those complexes. Thus, while the oxo-hydroxo forms of 5 and 7 are also present, they are contributing little to the overall rate. Alternatively, another pK_a could be compensating for the second (hydroxo to aqua) prototropic equilibrium that is apparent in the reactivity profiles of 5 and 7. We cannot distinguish between these kinetically equivalent scenarios with the data at hand.

The pronounced reactivity trend observed for these very similar oxo-Mn(V) porphyrins is opposite to what would be expected for the effect of electron withdrawing groups on the periphery of an oxidation catalyst. Usually, electron-deficient substituents would destabilize a high-valent metal complex making it more electrophilic and thus more reactive, as has been observed for manganese salen-mediated epoxidations [47]. We have attributed the reverse reactivity trend for the manganese pyridyl porphyrins to two main factors, increased acidity of the metal-coordinated water and a stabilization of the A_{2u} orbital in the oxo-aqua-Mn(V) species by the electron withdrawing group [34]. The latter effect results in an increase of the singlet–triplet–quintet excited state energy gaps as the electron-withdrawing effect of the porphyrin ligand increases. In fact, the A_{2u} orbital has large coefficients on both the porphyrin nitrogens and the *meso*-carbons. This orbital is then strongly affected by a change in substituents at the *meso*-positions. In a similar manner, the higher electron deficiency of the imidazolyl ligand should result in a higher stabilization of the A_{2u} orbital, and therefore a lower reactivity of the complex as is observed.

4.3. Equilibrium constants and redox potentials

The second-order rate constants k_{for} and k_{rev} , corresponding to the forward reaction ($\text{Mn(III)} + \text{HOBr/Br}^-$) and reverse reaction (oxo-Mn(V) + Br^-), have been determined for the imidazolyl, 2- and 4-pyridyl porphyrins [33] at various pH values. From these data, equilibrium constants K_{equi} corresponding to the oxygen transfer interconversion can be obtained. The equilibrium constants determined at pH 8 for all three complexes considered are gathered in Table 2. For all three complexes, K_{equi} values above 1 are found. These results show that at pH 8, the forward reaction (formation of the high-valent species) is favored compared to the reverse one (oxidation of bromide). The K_{equi} value for Mn[TDMImP] is about 2–3 orders of magnitude larger than for the 2- and 4-pyridyl porphyrins. This clearly shows that the oxidation to the high-valent oxo-Mn(V) complex by HOBr/OBr⁻ is facilitated by the highly electron withdrawing imidazolyl porphyrin at pH 8.

From the equilibrium constants determined for each porphyrin, E vs pH diagrams were constructed (Fig. 7) [33]. This plot indicates that the oxidation of bromide by the oxo-Mn(V) complexes is facilitated under acidic conditions as this reaction becomes thermodynamically more favorable. In the pH range investigated (5–8), the imidazolyl porphyrin has lower potentials than the two other porphyrins studied. The redox potential of oxo-Mn(V)/Mn(III) for the imidazolium porphyrin approaches that of $\text{H}_2\text{O}_2/\text{H}_2\text{O}$ at low pH. The potentials of the oxo-Mn(V)/Mn(III) couples are dependent on the pK_a values of both the Mn(III) and oxo-Mn(V) complexes. The imidazolyl porphyrin, being more acidic than the two other porphyrins considered, has lower pK_a values than the 2- and 4-pyridyl porphyrins. Thus, the higher acidity of the imidazolyl porphyrin is responsible for the lower reactivity of complex 2 at moderate and high pH.

Table 2
Equilibrium constants K_{equi} determined at pH 8 for the interconversion reaction for Mn[TDMImP], Mn[2-TMPyP] and Mn[4-TMPyP]

Porphyrin ligand	k_{for} ($\text{M}^{-1} \text{s}^{-1}$)	k_{rev} ($\text{M}^{-1} \text{s}^{-1}$)	K_{equi} ($k_{\text{for}}/k_{\text{rev}}$)
	Mn(III) + NaOBr	Mn(V) = O + NaBr	
TDMImP	1.65×10^6	1.43×10^3	1155
2-TMPyP	1.25×10^5	1.58×10^4	7.9
4-TMPyP	2.24×10^5	2×10^5	1.12

5. Conclusions

A fast, reversible oxygen atom transfer between bromide and the manganese *meso*-imidazolium porphyrin complex oxo-Mn(V)[TDMImP], (2), has been observed directly and compared to those previously observed with the 2- and 4-*N*-methylpyridyl porphyrin complexes. The oxygenation of bromide is favored at lower pH values while the reverse reaction between Mn(III)[TDMImP] (1) and BrO⁻ is accelerated as the pH is raised. Indeed, the rate of oxygen transfer of these oxo-Mn(V) complexes was observed to decrease by 3–5 orders of magnitude between pH 5 and pH 9. The slow reaction at high pH is attributed to the formation of a kinetically stable dioxo-Mn(V) complexes [O=Mn(V)=O]⁻. The initially-formed oxo-Mn(V) complex is observed to transform into the more stable oxo-Mn(IV) complex in a slower process that is dependent upon bromide. We conclude that the oxo-Mn(V) complex is in equilibrium with the corresponding Mn(III)-OBr adduct that undergoes homolytic MnO–Br bond cleavage to produce the oxo-Mn(IV) complex. A ΔG^0 of –6.5 kcal/mol was determined for this one-electron reduction of the oxo-Mn(V) complex with concomitant formation of a bromine atom. The potential vs pH diagram constructed for the oxo-Mn(V)/Mn(III) couple indicates that the imidazolyl porphyrin complex can reach higher potentials at low pH compared to the 2- and 4-pyridyl porphyrin complexes. This is a result of the higher acidity of this complex. The equilibrium constants observed for the reversible oxygen transfer from oxo-Mn(V) indicate that nearly all of the oxidizing power of HOBr is retained in the high-valent manganese complex. Therefore, the synthesis of even more electron-deficient manganese porphyrin complexes could increase the oxidation potential enabling the possible oxidation of water under acidic conditions.

The reader is referred to the following references for further thoughts on the dedication of this work [60,61].

6. Abbreviations

Mn(III)[TDMIm]Cl 5,10,15,20-tetrakis[1,3-*N,N*-dimethylimidazol-2-yl]porphyrinato manganese(III) chloride

Mn(III)[2-TMPyP]Cl 5,10,15,20-tetrakis[2-*N*-methylpyridyl]porphyrinato manganese(III) chloride

Mn(III)[4-TMPyP]Cl 5,10,15,20-tetrakis[4-*N*-methylpyridyl]porphyrinato manganese(III) chloride

BDE bond dissociation energy

NHE normal hydrogen electrode

S singlet state

T triplet state

Q quintet state

Acknowledgement

Support of this research by the National Science Foundation (CHE 0316301) is gratefully acknowledged.

Appendix A. Supplementary material

Supplementary data associated with this article can be found, in the online version, at doi:10.1016/j.jinorgbio.2007.07.017.

References

- [1] B. Meunier, S.P. de Visser, S. Shaik, Chem. Rev. 104 (2004) 3947–3980.
- [2] J.T. Groves, in: P.R. Ortiz de Montellano (Ed.), Cytochrome P450: Structure, Mechanism, and Biochemistry, third ed., Models and Mechanisms of Cytochrome P-450 action, Kluwer Academic/Plenum, New York, 2005, pp. 1–44 (Chapter 1).
- [3] I.G. Denisov, T.M. Makris, S.G. Sligar, I. Schlichting, Chem. Rev. 105 (2005) 2253–2327.
- [4] J.T. Groves, J. Inorg. Biochem. 100 (2006) 434–447.
- [5] T. Spolittak, J.H. Dawson, D.P. Ballou, J. Biol. Chem. 280 (2005) 20300–20309.
- [6] A. Butler, Coord. Chem. Rev. 187 (1999) 17–35.
- [7] T.L. Poulos, in: K.M. Kadish, K.M. Smith, R. Guilard (Eds.), The Porphyrin Handbook, Peroxidase and Cytochrome P450 Structures, Academic Press, San Diego, 2000, pp. 200–202 (Chapter 32).
- [8] A.G.J. Ligtenbarg, R. Hage, B.L. Feringa, Coord. Chem. Rev. 237 (2003) 89–101.
- [9] P. Ortiz-Bermudez, K.C. Hirth, E. Srebotnik, K.E. Hammel, Proc. Nat. Acad. Sci. USA 104 (2007) 3895–3900.
- [10] B.-A. Kaup, U. Piantini, M. Wust, J. Schrader, Appl. Microbiol. Biotechnol. 73 (2007) 1087–1096.
- [11] S.L. Neidleman, Biohalogenation: Principles, Basic Roles and Applications, Halsted Press, New York, 1986.
- [12] B.W. Griffin, in: J. Everse, K.M. Everse, M.B. Grisham (Eds.), Peroxidases in Chemistry and Biology, Chloroperoxidase: A Review, CRC Press, Boca Raton, FL, 1991, pp. 85–138 (Chapter 4).
- [13] M. Sundaramoorthy, J.M. Mauro, A.M. Sullivan, J. Terner, T.L. Poulos, Acta. Cryst. D 51 (1995) 842–844.
- [14] J.T. Groves, Proc. Nat. Acad. Sci. USA 100 (2003) 3569–3574.
- [15] W.-D. Woggon, Acc. Chem. Res. 38 (2005) 127–136.
- [16] J.A. Manthey, L.P. Hager, Biochemistry 28 (1989) 3052–3057.
- [17] A. Butler, J.V. Walker, Chem. Rev. 93 (1993) 1937–1944.
- [18] K. Kuhnelt, E. Derat, J. Terner, S. Shaik, I. Schlichting, Proc. Nat. Acad. Sci. USA 104 (2007) 99–104.
- [19] T. Egawa, H. Miki, T. Ogura, R. Makino, Y. Ishimura, T. Kitagawa, FEBS Lett. 305 (1992) 206–208.
- [20] K.L. Stone, R.K. Behan, M.T. Green, Proc. Nat. Acad. Sci. USA 102 (2005) 16563–16565.
- [21] H.-A. Wagenknecht, W.-D. Woggon, Chem. Biol. 4 (1997) 367–372.
- [22] H.-A. Wagenknecht, C. Claude, W.-D. Woggon, Helv. Chim. Acta 81 (1998) 1506–1520.
- [23] W.-D. Woggon, H.-A. Wagenknecht, C. Claude, J. Inorg. Biochem. 83 (2001) 289–300.
- [24] R.D. Libby, A.L. Shedd, A.K. Phipps, T.M. Beachy, S.M. Gerstberger, J. Biol. Chem. 267 (1992) 1769–1775.
- [25] S. Colonna, N. Gaggero, L. Casella, G. Carrea, P. Pasta, Tetrahedron Asymm. 3 (1992) 95–106.
- [26] E.J. Allain, L.P. Hager, L. Deng, E.N. Jacobsen, J. Am. Chem. Soc. 115 (1993) 4415–4416.
- [27] M. Hofrichter, R. Ullrich, Appl. Microbiol. Biotechnol. 71 (2006) 276–288.
- [28] K. Kuhnelt, W. Blankenfeldt, J. Terner, I. Schlichting, J. Biol. Chem. 281 (2006) 23990–23998.
- [29] I. Wilson, K.R. Bretscher, C.K. Chea, H.C. Kelly, J. Inorg. Biochem. 19 (1983) 345–357.
- [30] J.T. Groves, W.J. Kruper, R.C. Haushalter, J. Am. Chem. Soc. 102 (1980) 6375–6377.

- [31] J.T. Groves, Y. Watanabe, T.J. McMurry, *J. Am. Chem. Soc.* 105 (1983) 4489–4490.
- [32] G. Labat, B. Meunier, *J. Chem. Soc., Chem. Commun.* (1990) 1414–1416.
- [33] N. Jin, J.L. Bourassa, S.C. Tizio, J.T. Groves, *Angew. Chem. Int. Ed.* 39 (2000) 3849–3851.
- [34] F. De Angelis, N. Jin, R. Car, J.T. Groves, *Inorg. Chem.* 45 (2006) 4268–4276.
- [35] Y. Shimazaki, T. Nagano, H. Takesue, B.-H. Ye, F. Tani, Y. Naruta, *Angew. Chem. Int. Ed.* 43 (2004) 98–100.
- [36] M. Gazda, D.W. Margerum, *Inorg. Chem.* 33 (1994) 118–123.
- [37] D.H. Tjahjono, T. Akutsu, N. Yoshioka, H. Inoue, *Biochim. Biophys. Acta* 1472 (1999) 333–343.
- [38] J. Crapo, Patent WO 00/43395, 2000.
- [39] N. Jin, J.T. Groves, *J. Am. Chem. Soc.* 121 (1999) 2923–2924.
- [40] J.V. Walker, M. Morey, H. Carlsson, A. Davidson, G.D. Stucky, A. Butler, *J. Am. Chem. Soc.* 119 (1997) 6921–6922.
- [41] J.T. Groves, J. Lee, S.S. Marla, *J. Am. Chem. Soc.* 119 (1997) 6269–6273.
- [42] W. Nam, I. Kim, M.H. Lim, H.J. Choi, J.S. Lee, H.G. Jang, *Chem. Eur. J.* 8 (2002) 2067–2070.
- [43] R. Zhang, J.H. Horner, M. Newcomb, *J. Am. Chem. Soc.* 127 (2005) 6573–6582.
- [44] W.J. Song, M.S. Seo, G.S. DeBeer, T. Ohta, R. Song, M.-J. Kang, T. Tosha, T. Kitagawa, E.I. Solomon, W. Nam, *J. Am. Chem. Soc.* 129 (2007) 1268–1277.
- [45] Z. Gross, G. Golubkov, L. Simkhovich, *Angew. Chem. Int. Ed.* 39 (2000) 4045–4047.
- [46] D.E. Lansky, B. Mandimutsira, B. Ramdhanie, M. Clausen, J. Penner-Hahn, S.A. Zvyagin, J. Telsler, J. Krzystek, R. Zhan, Z. Ou, K.M. Kadish, L. Zakharov, A.L. Rheingold, D.P. Goldberg, *Inorg. Chem.* 44 (2005) 4485–4498.
- [47] M. Palucki, N.S. Finney, P.J. Pospisil, M.L. Guler, T. Ishida, E.N. Jacobsen, *J. Am. Chem. Soc.* 120 (1998) 948–954.
- [48] R.W. Lee, P.C. Nakagaki, T.C. Bruice, *J. Am. Chem. Soc.* 111 (1989) 1368–1372.
- [49] P.L. Anelli, S. Banfi, F. Legramandi, F. Montanari, G. Pozzi, S. Quici, *J. Chem. Soc. Perkin Trans I* (1993) 1345–1357.
- [50] M.-E. De Carvalho, B. Meunier, *Tetrahedron Lett.* 24 (1983) 3621–3624.
- [51] B. Meunier, E. Guilmet, M.-E. De Carvalho, R. Poilblanc, *J. Am. Chem. Soc.* 106 (1984) 6668–6676.
- [52] B. De Poorter, M. Ricci, O. Bortolini, B. Meunier, *J. Mol. Cat.* 31 (1985) 221–224.
- [53] O. Bortolini, M. Ricci, B. Meunier, P. Friant, I. Ascione, J. Goulon, *Nouv. J. Chem.* 10 (1986) 39.
- [54] J.A. Kerr, in: D.R. Lide (Ed.), *Handbook of Chemistry and Physics*, 84th ed., CRC Press, Boca Raton, 2003.
- [55] L. Huang, P.R. Ortiz de Montellano, *Biochem. Biophys. Res. Commun.* 355 (2007) 581–586.
- [56] V.E. Tumanov, E.T. Denisov, *Kinet. Catal.* 45 (2004) 661–667.
- [57] D.M. Stanbury, *Adv. Inorg. Chem.* 33 (1989) 69–138.
- [58] M. Hung, A. Bakac, *Inorg. Chem.* 44 (2005) 9293–9298.
- [59] F.C. Chen, S.H. Cheng, C.H. Yu, M.H. Liu, Y.O. Su, *J. Electroanal. Chem.* 474 (1999) 52–59.
- [60] F.M.M. Morel, J.T. Groves, *Science* 314 (2006) 1406.
- [61] G.C. Dismukes, M. Hecht, T.G. Spiro, J.T. Groves, R.R. Chianelli, *J. Inorg. Biochem.* 101 (2007) vii–viii.